Molecular Dynamics and Free Energy Studies on the Wild-type and Double Mutant HIV-1 Protease Complexed with Amprenavir and Two Amprenavir-Related Inhibitors: Mechanism for Binding and Drug Resistance

Tingjun Hou* and Ron Yu

Center for Theoretical Biological Physics, University of California at San Diego, 9500 Gilman Drive, La Jolla, California 92093-0319

Received July 31, 2006

The V82F/I84V double mutation is considered as the key residue mutation of the HIV-1 protease drug resistance because it can significantly lower the binding affinity of protease inhibitors in clinical uses. In the current work, the binding of amprenavir to both of the wild-type and the drug-resistant V82F/I84V mutant of the HIV-1 protease was investigated by molecular dynamics (MD) simulations and was compared to those of two inhibitors in development, TMC126 and TMC114. Absolute binding free energies were calculated by molecular mechanics/Poisson−Boltzmann surface area (MM/ PBSA) methodology. The predicted binding affinities give a good explanation of structure−affinity relationship (SAR) of three studied inhibitors. Furthermore, in the 18 ns MD simulations on the free wild-type and the mutated proteases, we observed that the free mutated protease shows similar dynamic characteristics of the flap opening and a little higher structural stability than the free wild-type protease. This suggests that the effect of the mutations may not significantly affect the equilibrium between the semiopen and the closed conformations. Finally, decomposition analysis of binding free energies and the further structural analysis indicate that the dominating effect of the V82F/I84V double mutation is to distort the geometry of the binding site and hence weaken the interactions of inhibitors preshaped to the wild-type binding site.

Introduction

The human immunodeficiency virus type I aspartic protease (HIV-1 protease) is one of the most important enzymes in anti-AIDS drug design.[1] This viral protein cleaves the *gag* and *pol* nonfunctional polypeptide into functional proteins essential for maturation of infectious HIV particles.[2] Inactivation of this enzyme causes the production of immature, noninfectious viral particles and hence blocks further HIV infection. HIV protease consists of two identical 99 amino acid monomers forming a homodimer with a central symmetric, substrate-binding cavity.[3−5] As a member of the aspartyl protease family, the HIV-1 protease is composed of conserved residues, the so-called binding triads: D25(D25′)-T26(T26′)-G27(G27′), of which D25 and D25′ are known to be active residues.

Eight antiviral agents that can inhibit HIV-1 protease have been approved by the Food and Drug Administration (FDA), including saquinavir, ritonavir, indinavir, nelfinavir, amprenavir, lopnavir, atazanavir, and tipranavir, with several others under clinical investigation.[6] Although numerous studies have led to the discovery and development of numerous HIV-1 protease inhibitors, a "perfect" protease drug seems far from us, because therapeutic benefit is short-lived and treatment success is usually limited due to the evolution of drug-resistance variants.[7,8] Resistance to protease inhibitors is the consequence of amino acid substitutions that emerge either inside the substrate-binding pocket or at distant sites. On the molecular level, resistance is primarily caused by a dramatic decrease in the affinity of the inhibitor for protease mutants, while the binding of the substrates is not as heavily affected. More than 20 mutations, located in the active site, the flap region, dimerization interface, and double-strand β-sheet, have been identified in clinical and *in vitro* isolates exposed to protease inhibitors.[8] Among all these mutations, the mutations of six residues can confer resistance to almost all protease drugs, including L10, M46, I54, V82, I84, and L90, which are located in different regions of protease, including the active site (V82 and I84), the flap region (M46 and I54), and the dimerization interface (L10 and L90).[9] The mutations of V82 and I84 in the active site have more significant effect on the binding affinities than the other four residues.[10,11] The double mutation of V82 and I84 impair affinities of all available drugs significantly. For example, the V82F/I84V double mutant has a 700-fold increase in K_i for ritonavir, 100-fold increase in K_i for amprenavir, a 79-fold increase in K_i for indinavir, 86-fold increase in K_i for nelfinavir, and 19-fold increase in K_i for saquinavir.[11]

Amprenavir (APV, **1**, Figure 1), a novel hydroxyethylamine sulfonamide, is a second-generation drug.[2,12] **1** was proved to be of high potency in combination therapies, had good bioavailability, and was well tolerated.[13] Although **1** shows high potency to most drug-resistant variants, significant resistance to **1** has still been observed when mutation occurs at several positions, including V82/I84 double mutation.[14−16] Based on the structure of **1**, a lead optimization program initially produced a series of bis-tetrahydrofuranyl compounds of which **2** (TMC126, Figure 1) was studied as the prototype.[17] **2** contains a tetrahydrofuranyl moiety and a sulfonamide isostere,[17] with extreme inhibition against a wide spectrum of protease variants.[18] Further optimization of the series resulted in the selection of **3** (TMC114, Figure 1) due to its superior pharmacokinetics and antiviral profile in comparison with all the other compounds of this series.[16] The structures of **1**, **2**, and **3** are quite similar (Figure 1), but why do they demonstrate different binding affinities with protease and different sensitivities to the V82F/I84V double mutation? In order to answer this question, nanosecond-level molecular dynamics (MD) simulations and free energy calculations were employed to access information about binding of **1**, **2**, and **3** to the wild-type protease and the V82F/I84V double

* To whom correspondence should be addressed. E-mail: tingjunhou@hotmail.com or tihou@ucsd.edu. Phone: 858-822-4596. Fax: 858-822-4236.

10.1021/jm0609162 CCC: $37.00
Published on Web 02/15/2007

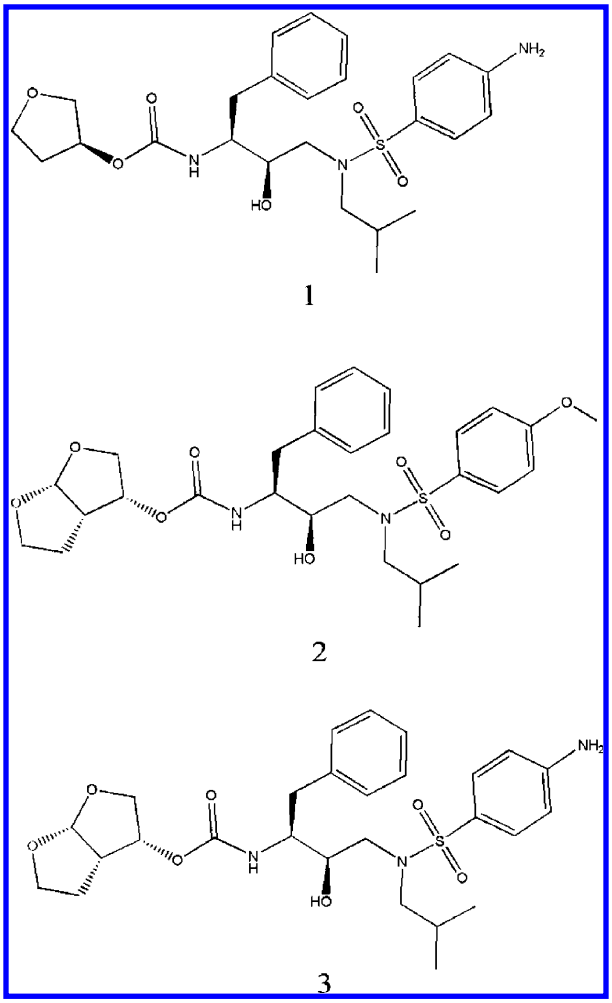

Figure 1. Chemical structures of **1**, **2**, and **3**.

mutant. Absolute binding free energy calculations were performed using the molecular mechanics/Possion−Boltzmann surface area (MM/PBSA) methodology.[19−26] In order to check the influence of the V82F/I84V double mutation on the dynamics characteristics of the unbound protease, 18 ns MD simulations were performed to the unbound wild-type and the unbound mutated proteases, respectively. According to the analyses of the structural fluctuation and the conformational change caused by mutations, as well as the calculations of the absolute binding free energy and the inhibitor−residue interaction spectrums, we expect that the following three aims can be achieved: (1) Understand the difference between the mechanisms of **1**, **2**, and **3** binding to the wild-type protease. (2) Obtain information of the influence of the V82F/I84V double mutation to the dynamic properties of the unbound protease. (3) Estimate the influence of binding of **1**, **2**, and **3** caused by the V82F/I84V double mutation, and hypothesize the molecular mechanisms for HIV-1 drug resistance caused by the V82F/I84V double mutation.

Materials and Methods

1. Initial Structures. The starting structures and force-field parameters for the inhibitors were obtained as follows: first, hydrogen atoms were added to the X-ray coordinates of **1** extracted from the HIV-1 protease/**1** crystal complex (PDB entry: 1hpv),[27] and **2** and **3** were obtained by modifying the structure of **1**. Then, the atom partial charges of **1**, **2**, and **3** were derived by semiempirical AM1 geometry optimization and subsequent single-point Hartree−Fock (HF)/6-31G* calculations of the electrostatic potential, to which the charges were fitted using the RESP fitting technique.[28] The optimization and electrostatic potentials calculation were finished using Gaussian 98.[29] Partial charges and force field parameters for the inhibitors were generated automatically using the Antechamber program in AMBER8.0.[30]

The crystal structure of the HIV-1 protease/**1** complex was taken as the starting point for MD simulations of the complexes. All missing hydrogen atoms of the protein were added using the Xleap program in AMBER8.0.[30] Special attention was given to the protonation state of Asp25 and Asp25′ in the active site because they occur in three possible states (diprotonated, monoprotonated, and deprotonated) depending on the inhibitor bound.[31−34]. So protonation of D25/D25′ was assigned into six different ionizable states, including unprotonation, four monoprotonated states for D25′ or D25, and diprotonation. The two Asp25 residues in protease can adopt two possible configurations, labeled as "up" and "down" based on the position of proton on OD1 oxygen or OD2 oxygen atom of D25 or D25′, as illustrated in Figure S1 in the Supporting Information. Here, the protonation states were labeled as unpro, mono25_down, mon25_up, mono25′_down, mon25′_up and dipro, respectively (see Figure S1 in the Supporting Information). The mono25_up model was adopted in the current work. Determination of the protonation state can be found in the Supporting Information.

The initial structures of **2** and **3** complexed with the wild-type HIV-1 protease were obtained by modifying the structure of **1** in the crystal structure of 1hpv. Then the mutating process of Val82 and Ile84 to Phe82 and Val84 was accomplished using the SYBYL molecular simulation package to obtain three double-mutated complexes.[35] A total of eleven systems, including three wild-type protease complexes, three mutated protease complexes, one unbound wild-type protease, one unbound mutated protease, and three free inhibitors, were simulated here. The unbound wild-type and the mutated proteases were obtained by deleting the inhibitors from the active site. In the following molecular mechanics (MM) minimizations and molecular dynamics (MD) simulations, AMBER03 force field was used to establish the potentials of proteins,[36] and general AMBER force field (gaff) was used to establish the potentials of inhibitors.[37] To neutralize the charge of the systems, counterions of Cl^- were placed to grids with the largest positive Coulombic potentials around protease, and then the whole system was immersed in the rectangular box of TIP3P water molecules.[38] The water box extended 10 Å away from any solute atoms.

2. Molecular Dynamics (MD) Simulations. In molecular minimization and molecular dynamics simulations, particle mesh Ewald (PME) was employed to treat the long-range electrostatic interactions.[39] Before MD simulations, the protease complexes and the free protease systems were gradually relaxed using 10 000 cycles of minimization procedure (500 cycles of steepest descent and 9500 cycles of conjugate gradient minimization). After minimization, MD simulations in the NPT ensemble with a target temperature of 300 K and a target pressure of 1 atm were performed. The SHAKE procedure was employed to constrain all hydrogen atoms,[40] and the time step was set to 2.0 fs. Before the actual MD simulations, the system was gradually heated in the NVT ensemble from 10 K to 300 K over 20 ps. Initial velocities were assigned from a Maxwellian distribution at the starting temperature. MD samplings at 1.5, 18, and 2 ns were performed for complexes, the free proteases, and the free inhibitors, respectively. During the sampling process, coordinates were saved every 2 ps in the simulations of the complexes and the free proteases, and every 10 ps for the free inhibitors.

3. MM/PBSA Calculations. The absolute binding free energy ($\Delta G_{binding}$) was calculated using the MM/ PBSA procedure according to:

$$\Delta G_{binding} = \langle G^{complex}(i)\rangle_i - \langle G^{protein}(i)\rangle_i - \langle G^{inhibitor}(i)\rangle_i \quad (1)$$

where $\langle G^{complex}(i)\rangle_i$, $\langle G^{protein}(i)\rangle_i$, and $\langle G^{inhibitor}(i)\rangle_i$ represent the free energies of complex, protein, and inhibitor averaged over snapshots i taken from MD trajectories, and $G^x(i)$ is estimated by summing

the contributions of gas-phase energies, solvation free energy, and entropies (see eq 2)

$$G^x(i) = H^x_{gas}(i) + G^x_{solvation}(i) - TS^x(i) \quad (2)$$

If the predictions of free energies of complex, protein, and inhibitor are based on snapshots taken from a single trajectory of the complex (single trajectory protocol), the binding free energy is predicted as:

$$\Delta G_{binding} = \langle G^{complex}(i) - G^{protein}(i) - G^{inhibitor}(i)\rangle_i \quad (3)$$

The gas-phase energies H_{gas} of the solute denote the sum of molecular mechanical (MM) energies of the molecules from internal, electrostatic, and van der Waals energies. The solvation free energy $G_{solvation}$ is computed as the sum of polar (G_{polar}) and nonpolar ($G_{nonpolar}$) parts. Here, the polar contribution was calculated by solving the Poisson−Boltzmann (PB) equations for nonzero salt concentrations as implemented in Delphi II.[41] In Delphi calculations, the grid spacing was set to 0.5 Å, and the radii of atoms were taken from the PARSE parameter set.[42] The values of the interior dielectric constant and the exterior dielectric constant were set to 2 and 80, respectively. The nonpolar contribution was determined based on solvent-accessible surface area determined with the LCPO method:[43] $G^x_{nonpolar}(i) = 0.0072 \times SASA^x(i)$. For the calculations of H_{gas}, G_{polar}, and $G_{nonpolar}$, 160 snapshots from 0.2 to 1.5 ns were extracted from the single trajectory of complex at time intervals of about 8 ps. The normal-mode analysis was performed to estimate the conformational entropy upon ligand binding using the *nmode* program in AMBER8.0.[30] Each snapshot was fully minimized for 100 000 steps in the presence of a distance-dependent dielectric of $4r_{ij}$ (r_{ij} is the distance between two atoms) until the root-mean-square of the elements of the gradient vector was less than 5×10^{-5} kcal mol^{-1} Å^{-1}. Due to the high computational demand, only 25 snapshots were used to estimate the contribution of the entropies of association.

4. Inhibitor−Residue Interaction Decomposition. Due to the high computational demand of PB calculations, the interaction between each inhibitor and each protease residue was computed using the MM/GBSA decomposition process applied in the *mm_pbsa* module in AMBER8.0. The binding interaction of each inhibitor−residue pair includes three terms: van der Waals contribution (ΔG_{vdw}), electrostatic contribution (ΔG_{ele}), and solvation contribution ($\Delta G_{solvation}$).

$$\Delta G_{inhibitor\_residue} = \Delta G_{vdw} + \Delta G_{ele} + \Delta G_{GB} \quad (4)$$

where ΔG_{vdw} and ΔG_{ele} are nonbonded van der Waal interaction and electrostatic interaction between inhibitor and each protease residue, which can be computed using the *sander* program in AMBER8.0. The polar contribution (ΔG_{GB}) of $\Delta G_{solvation}$ was computed using the generalized Born model, and the parameters for GB calculations were developed by Onufriev et al.[44] The charges used in GB calculations were taken from the AMBER parameter set. All energy components in eq 4 were calculated using 50 snapshots from 0.2 to 1.5 ns.

Results and Discussion

(i) Stability and Flexibility of the Wild-type Protease Complexes. To explore the dynamic stability of three wild-type protease/drug complexes, root-mean-square displacement (rmsd) values for the protease C_α atoms during the production phase relative to the starting structures were calculated and plotted in Figure 2. The rmsd plots indicate that the conformations of the **2** and **3** complexes achieve equilibrium much faster than that of the **1** complex. The **1** trajectory still does not reach good equilibrium until about 700 ps, while the **2** and the **3** trajectories are stable after about 600 ps. Moreover, the rmsd fluctuation of the **1** complex is very significant, indicated by the larger standard deviation (SD) of rmsd of the **1** trajectory (0.156) than those of the **2** (0.078) and the **3** (0.075) trajectories (the calculation of SD of rmsd was based on the snapshots from 700 ps to 1.5 ns).

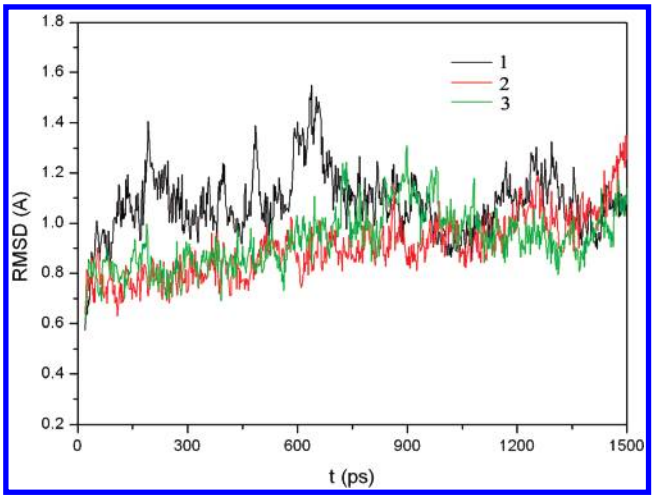

Figure 2. Root-mean-square displacement (rmsd) of the backbone C_α atoms of the wild-type HIV-1 protease/**1** complex, the wild-type HIV-1 protease/**2** complex, and the wild-type HIV-1 protease/**3** complex with respect to the first snapshot as a function of time.

Detailed analysis of root-mean-square fluctuation (rmsf) versus the residue number for three complexes is illustrated in Figure 3. Overall, the three structures share similar rmsf distributions. The average rmsf per residue for the **1**, **2**, and **3** complexes are 0.67, 0.61, and 0.61, respectively. The relatively larger rmsf per residue of the **1** complex may be explained by the relatively weaker binding of **1**. Three complexes display similar trends of dynamic features. Regions around Asp25 and Asp25′ show a rigid behavior, which is in agreement with experiments[45] and theoretical studies.[46] Besides the N- and C-terminal residues, four regions around 16(17′), 40(40′), 53-(53′), 68(68′), 81(81′) show the greatest dynamic fluctuations. The whole flap region (residues 38−58), especially the flap elbow region (residues 37−42), shows high flexibility. This result well agrees with a recent study, where the authors also determined these regions of largest flexibility based on the differences in the crystal structures in combination with MD results.[47] As shown in Figure S3 in the Supporting Information, the flexibility of the unbound protease is much greater than that of the **1**/PR complex, especially in the flap regions. This observation can be easily explained in terms of binding between protease and inhibitor that leads directly to the rigidity of the complex. This observation is also consistent with the work reported by Zhu et al.[48] They found that the strong hydrophobic interaction between the fullerene-based inhibitor and the flaps would cause the tight closing of the flexible flaps. It should be noted that in MD simulations, the crystallographic water which bridges the drug and Ile50/Ile50′ was included in the initial model. The bridge water was observed to be well maintained throughout the whole MD simulation.

(ii) Binding of 1, 2, and 3. In MM/PBSA calculations, the affinity of a ligand binding to a protein can be estimated by two protocols: (a) evaluate all terms using separate trajectories of complex, protein, and ligand (separate-trajectory protocol) or (b) just the snapshots from a trajectory of the complex (single-trajectory protocol). The single-trajectory protocol is much faster than the separate-trajectory protocol and potentially requires less sampling because all of the intramolecular energies cancel when calculating the association energy. Here we systematically compared the predictions using these two protocols. Moreover,

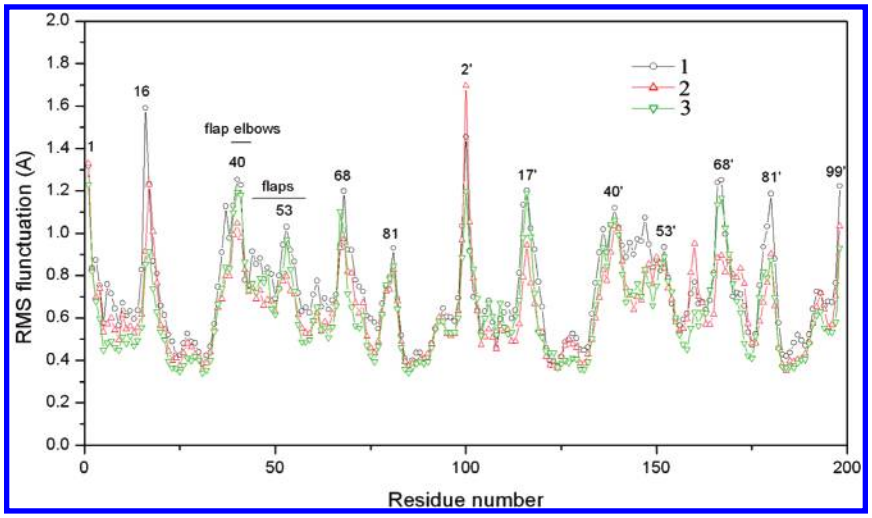

Figure 3. Root-mean-square fluctuation of backbone atoms versus residue number of the wild-type HIV-1 protease/**1** complex, the wild-type HIV-1 protease/**2** complex, and the wild-type HIV-1 protease/**3** complex.

Table 1. Binding Free Energies of **1**, **2**, and **3** Complexed with the Wild-type (WT) Protease or the Mutated Protease (kcal/mol)

ligand	protease	ΔE_{ele}	ΔE_{vdw}	ΔG_{SA}	ΔG_{PB}	$-T\Delta S$	$\Delta G_{pred}{}^a$	$\Delta G_{pred}{}^b$	ΔG_{exp}
1	WT	−24.13	−62.22	−7.02	47.15	26.20	−46.22	−20.02	−13.2
	protease	(2.47)	(3.66)	(0.16)	(3.63)	(6.85)			
	mutated	−19.55	−59.57	−6.94	43.57	25.47	−42.49	−17.02	−10.5
	protease	(3.12)	(3.44)	(0.12)	(3.74)	(7.38)			
2	WT	−20.94	−66.46	−7.37	45.54	23.31	−49.22	−25.91	−15.6
	protease	(3.08)	(3.64)	(0.13)	(3.22)	(7.24)			
	mutated	−19.51	−66.18	−7.34	45.84	25.64	−47.21	−21.57	−14.1
	protease	(2.17)	(3.14)	(0.11)	(2.61)	(6.67)			
3	WT	−25.60	−68.50	−7.09	53.87	25.51	−47.31	−21.80	−15.2
	protease	(2.64)	(3.98)	(0.10)	(3.53)	(7.57)			
	mutated	−19.51	−63.11	−7.08	45.84	23.34	−43.86	−20.54	
	protease	(2.71)	(3.87)	(0.12)	(3.39)	(5.58)			

[a] The predictions do not include entropy effect. [b] The predictions include entropy effect.

the influence of different length of conformational sampling was also investigated. The detailed descriptions of the comparison of these two different protocols are shown in the Supporting Information. Considering the high stability of prediction, the single-trajectory protocol was used in the following studies.

Absolute binding free energies of **1**, **2**, and **3** using the single-trajectory protocol are shown in Table 1. The predicted binding free energies of **1**, **2**, and **3** are −20.02, −25.91, and −21.80 kcal/mol, respectively. According to the energy components of the binding free energies (Table 1), the major favorable contributors to ligand binding are van der Waals and electrostatic terms, whereas polar solvation and entropy terms oppose binding. Nonpolar solvation terms, which correspond to the burial of SASA upon binding, contribute slightly favorably. Furthermore, it is so encouraging that the experimental rank of the experimental affinity of **1**, **2**, and **3** (−13.2, −15.6, and −15.2 kcal/mol)[49,50] is consistent with our predictions.

In order to gain a detailed picture of the binding energetics, binding free energy was decomposed into ligand−residue pairs and shown in Figure 4. The quantitative information is extremely useful to the understanding of binding mechanism for an inhibitor/PR complex. Overall, the interaction spectrums of the three drugs are quite similar. The favorable residues can be classified into six clusters around residues A28, I50, I84, A28′, I50′, and I84′. The geometries of six residues in the protease/**1** complex that have the largest contribution to the **1**, **2**, and **3** binding based on the interaction spectrum in Figure 4 are shown in Figure S4 in the Supporting Information. It is interesting to find that all those important residues are hydrophobic, which can form strong van der Waals interactions with the inhibitors. One observation of the energy decomposition analysis is the binding of drugs to the A chain is similar to the B chain. For example, the linear correlation coefficient between the interactions of **1** with each residue in monomer A and those of **1** with each residue in monomer B is 0.98. Even only considering the residue within 8 Å of inhibitor **1**, the linear correlation is also very high (0.97). Although the inhibitors studied here are not symmetric molecules, their binding interactions with monomer A and with monomer B are nearly identical. Our calculations are not consistent with the calculation results reported by Zhang et al.[51] In Zhang's work, the authors applied the MFCC (molecular fractionation with conjugate caps) method to produce quantum mechanical interaction spectrums for six protease drug binding complexes and found the binding energy of **1** binding to monomer A (−67.87 kcal/mol) to be much stronger than that of **1** binding to monomer B (−50.42 kcal/mol). Moreover, the interaction spectrums obtained by Zhang et al. are quite different from those obtained here. According to the interaction spectrums reported by Zhang et al., the charged Asp25 can form stronger interactions with inhibitor than the other residues. But according to our prediction, the interaction between **1** and Asp25 is not so strong (Figure 4). We believe that ignoring the solvation effect may cause the significant difference between the binding energies of **1** with two monomers reported by Zhang et al. For example, the electrostatic interaction between **1** and Asp25 is very strong (−4.92 kcal), but the interaction between **1** and Asp25 is significantly reduced when ΔE_{ele} and ΔG_{PB} (3.42 kcal/mol) are summed together.

Among these three inhibitors, **2** can produce the strongest affinity with protease. Further analysis of energy contribution

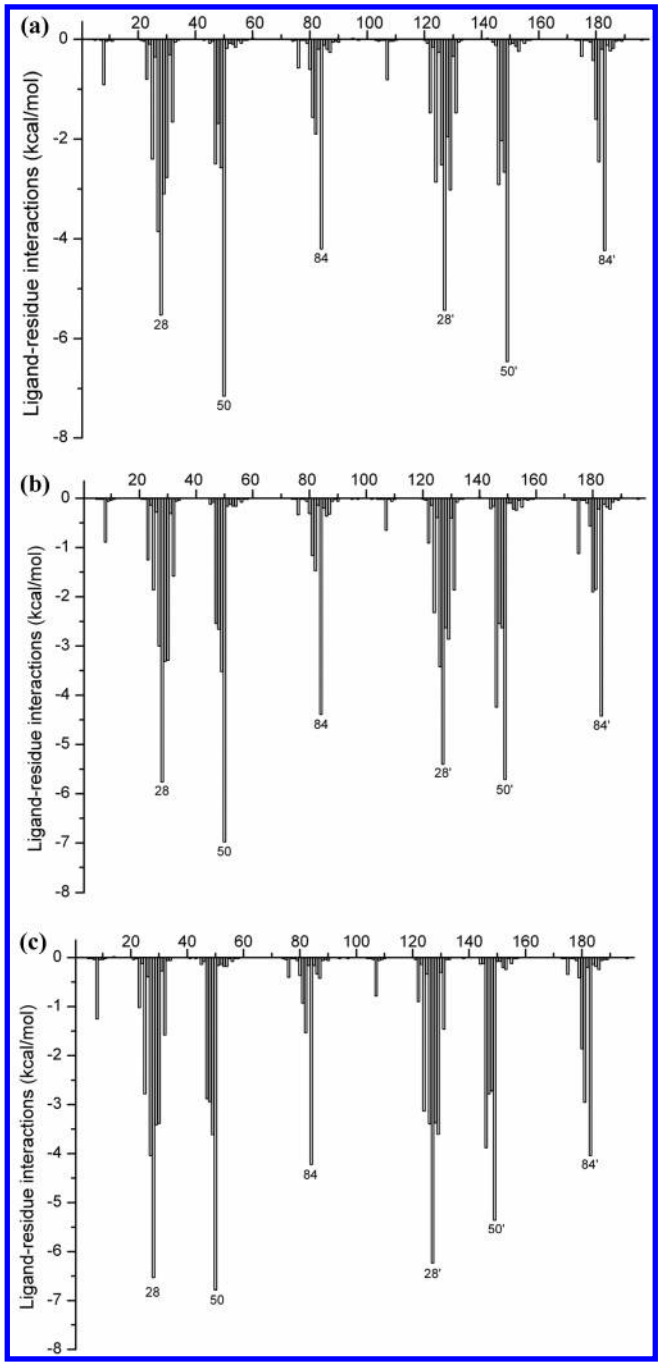

Figure 4. Ligand−residue interaction spectrum of (a) the HIV-1 protease/**1** complex, (b) the HIV-1 protease/**2** complex, and (c) the HIV-1 protease/**3** complex according to the MM/GBSA method. The *x*-axis denotes the residue number of PR and the *y*-axis denotes the interaction energy between the inhibitor and specific residues.

shows that the van der Waals interaction between **2** (−68.50 kcal/mol) and protease is stronger than that between **1** (−62.22 kcal/mol) and protease. Systematic analysis was performed to compare the difference between the inhibitor−residue interaction spectrum of **1** and that of **2**. According to analysis, we can find that there are 10 residues with the absolute value of difference larger than 0.40 kcal/mol, among which eight have stronger van der Waals interactions with **2** than with **1** and only two have stronger van der Waals interactions with **1** than with **2**. The spatial distribution of these ten residues is shown in Figure 5a. The eight residues favorable to **2** binding are located near the bicyclic tetrahydrofuran and the 4-methoxybenzenesulfonamide moieties. The larger fused bicyclic tetrahydrofuran group in **2**

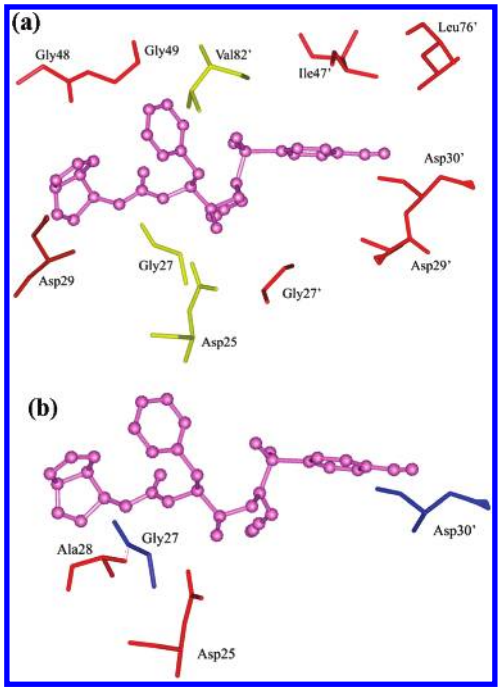

Figure 5. (a) Geometries of ten residues that contribute most to the difference between the van der Waals interaction of **1** and that of **2**. The residues with stronger van der Waals interaction with **2** are colored in red, and those with weaker van der Waals interaction with **2** in yellow. (b) Geometries of four residues that contribute most to the difference between the electrostatic interaction and the polar contribution of solvation of **1** and those of **2**. The residues with the stronger electrostatic interaction and polar contribution of solvation with **2** are colored in red, and those with the weaker in blue. The structure of **2** is shown in purple ball-and-stick model.

can produce better ligand−receptor van der Waals contacts. Moreover, the hydrophobic methoxyl group can also produce better van der Waals interaction with the surrounding residues, especially I47′. Quite different from the van der waals interaction, the electrostatic interaction between **1** and protease (−24.13 kcal/mol) is favorable than that between **2** and protease (−20.94 kcal/mol), but it should be noted that the polar interaction between **1** and protease is effectively reduced when ΔE_{ele} and ΔG_{PB} are summed together because **1** has more unfavorable polar contribution of desolvation (47.15 kcal/mol). The comparison of the electrostatic interaction between each residue and **1** and that between each residue and **2** shows that there are four important residues (Asp25, Gly27, Ala28, and Asp30′) contributing most to the difference between the electrostatic interaction and the polar contribution of solvation of **1** and those of **2** (Figure 5b). From the absolute values of differences, Asp25 and Asp30′ are more critical than the other two residues. In the average structure of the **1**/PR complex, the nitrogen atom in 4-aminobenzene of **1** can form two hydrogen bonds with Asp30′.

According to the predicted values, the binding of **3** is weaker than that of **2**, but stronger than that of **1**. The energy component analysis shows that both of the van der Waals interaction (−68.50 kcal/mol) and the electrostatic interaction (−25.60 kcal/mol) between **3** and protease are stronger than those (−62.22 and −24.13 kcal/ mol) between **1** and protease and those (−66.46 and −20.94 kcal/mol) between **2** and protease. But because of the high expense of the polar part of solvation, the binding of **3** (−47.31 kcal/mol) is weaker than that of **2** (−49.22 kcal/mol). The van der Waals interaction spectrums of **1** and **3** were compared. Totally, there are 16 residues with differences larger than 0.4 kcal/mol, among which 13 residues produce stronger van der Waals interaction with **3** than with **1** and the

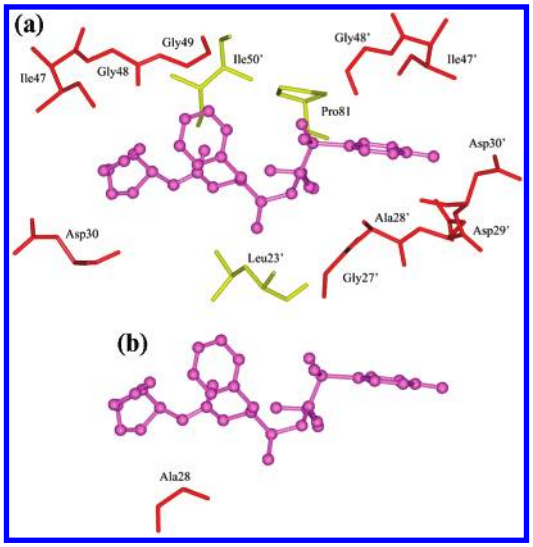

Figure 6. (a) Geometries of ten residues that contribute most to the difference between the van der Waals interaction of **1** and that of **3**. The residues with stronger van der Waals interaction with **3** are colored in red, and those with weaker van der Waals interaction with **3** in yellow. (b) Geometries of four residues that contribute most to the difference between the electrostatic interaction and the polar contribution of solvation of **1** and that of **3**. The residues with the stronger electrostatic interaction and polar contribution of solvation with **3** are colored in red, and those with the weaker in blue. The structure of **3** is shown in purple ball-and-stick model.

other 3 residues produce stronger van der Waals interactions with **1** than with **3**. The spatial distribution of these 16 residues is shown in Figure 6. It is interesting to find that the residues favorable to the binding of **3** are located near the fused bicyclic tetrahydrofuran and the 4-aminobenzene groups. It seems that the substitution of tetrahydrofuran in **1** to the fused bicyclic tetrahydrofuran group in **3** leads to the overall better van der Waals contact of **3**.

(iii) The Stability of the Wild-type and the Mutated Proteases. There are some published works indicating that some active-site mutations affect the dynamics and/ or the conformation of HIV-1 protease.[52−54] In 2002, Perryman et al. reported the MD simulations of a wild-type and the V82F/I84V mutant of HIV-1 protease.[55] The simulations show that more frequent and more rapid curling of the mutant's active site flaps was observed. Moreover, the mutant protease's flaps also open further than the wild-type's flaps and display more flexibility. So the authors concluded that the effect of the mutations on the equilibrium between the semiopen and closed conformations could be one aspect of the mechanism of drug resistance. Now, we performed two 18 ns MD simulations on the wild-type and the V82F/I84V double-mutated proteases. Although both systems depart from the same crystal structure with the closed form, they show different rmsd distributions as seen in Figure 7. At the first 3 ns stage, the mutant has a little larger rmsd than the wild-type protease. But after 4.5 ns, rmsd of the wild-type protease increases from about 1.4 Å to 1.8 Å, while that of the mutant decreases to 1.2 Å. At the high rmsd plateau of about 1.8 Å, the wild-type protease holds about 3.6 ns and then gradually decreases to rmsd of approximately 1.5 Å. The whole stage of rmsd increasing from 1.3 Å to 1.8 Å, staggering at 1.8 Å, and decreasing from 1.8 Å to 1.5 Å spends about 9 ns. After 9 ns, the structure of the wild-type protease reaches the stable conformational space although the fluctuation of rmsd is still significant. Compared with the wild-type protease, the rmsd fluctuation of mutant is quite different. After about 5 ns of high fluctuation, rmsd of the mutant becomes relatively stable. Moreover, the conformations of the mutant during MD simulations are quite closer to the crystal structure rather than those of the wild-type protease. The rmsd standard deviations of the wild-type protease and the mutated protease are 0.27 and 0.16, respectively, which means that the mutated protease may be more stable. The stabilities of the wild-type and the mutated proteases are further compared based on the rmsf values of each residue (Figure 8). The average rmsf value per residue of the wild-type protease is about 0.07 larger than that of the mutated protease, demonstrating that the wild-type protease has larger overall flexibility than the mutated protease.

It is well-known that the curling of the tips of the active site flaps triggers the opening of the entire flaps. The simulations reported by Rick et al.[55] show that the flap's tips curl in (residues 48−52 undergo large change in their ϕ and ψ torsion values and fold back onto themselves to give a bent L structure) before they open. Furthermore, the NMD data reported by Freedberg et al. demonstrates that the flap tip residues 49−53 bear significant motion occurring on a subnanosecond scale.[56] In Perryman's work, the authors investigated the distribution of the "TriCa angle" (the angle formed by three C_α atoms of three adjacent residues) formed by G48, G49, and I50, and observed that during 0−8 ns the G48-G49-I50 TriCa of the mutated protease switched frequently between ∼115° and ∼145° while the wild-type protease did not switch so frequently. Thus, the V82F/I84V mutated protease's flap tip curls more rapidly and more frequently than the wild-type's flap tip. Here, we also investigated the distributions of two TriCa angles (angle G48-G49-I50 and angle G48′-G49′-I50′). As seen in Figure 9, the distributions of the two angles (G48-G49-I50) do not show significant difference, but the G48′-G49′-I50′ triCa angle of the mutated protease spends more time at low values during 15−18 ns than that of the wild-type protease. The G48′-G49′-I50′ triCa angle of the mutated protease shows a broader distribution, and its mean value is about 135°, which is about 5° larger than that of the G48′-G49′-I50′ triC_α angle of the wild-type protease.

In order to investigate the extent of flap opening in MD simulations, the distance between the flap tip (I50 and I50′) and the catalytic Asp residues (D25 and D25′) was calculated. The measure of the I50−D25 or the I50′−D25′ distance (the distance between C_α of I50/I50′ and that of D25/D25′) was believed to be more reasonable than the measure by monitoring the tip−tip (I50−I50′) distance, because the tip−tip distance can be affected by both flap tip curling and by flap asymmetry.[54] The distributions of the I50−D25 and I50′−D25′ distances are shown in Figure 10. Comparing the motions of two flaps (Figure 10a and 10b) shows that the two flaps may move independently because at each snapshot the two distances in two monomers show a large difference. Previous MD simulations carried out by Scott et al. demonstrated that the flaps behaved asymmetrically at any one point of time even if the MD simulation was based on a perfectly symmetrical *apo* HIV-1 protease structure.[57] Detailed analysis of Figure 10a shows that the mutant's flap in monomer A opens more than the wild-type's flap in the former simulation part (0 to 8 ns) while opens less in the later part (8 to 18 ns). As shown in Figure 10b, in most parts of simulations, the mutant's flap and the wild-type's flap in monomer B show similar opening, while from 2 to 4.5 ns the wild-type's flap in monomer B shows larger opening and after 13.5 ns the mutant's flap in monomer B shows larger opening. In order to take a complete consideration of the opening extent of two flaps, the distributions of the I50−D25 distance and the I50′−D25′ distance were averaged and shown in Figure 10c. An interesting finding is that the standard deviations (SD) of the distributions

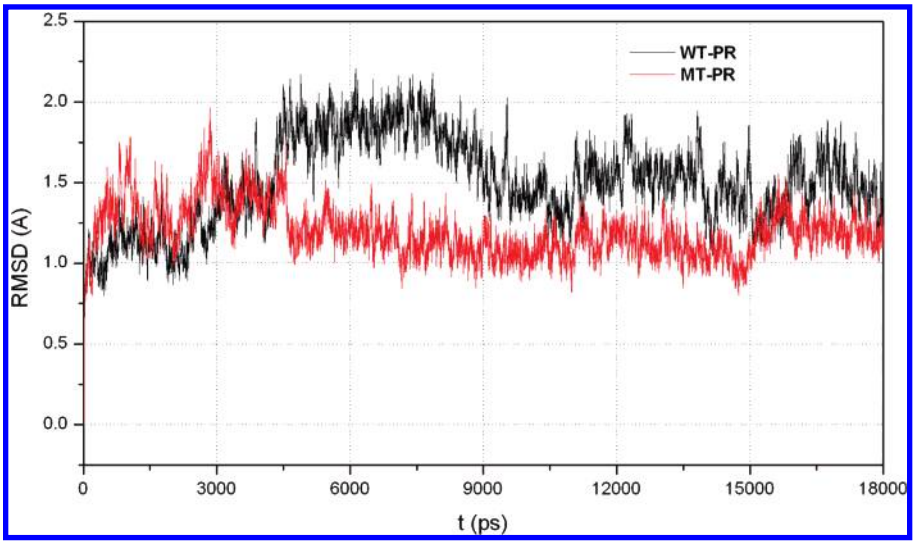

Figure 7. Root-mean-square displacement (rmsd) of the backbone C_α atoms of the unbound wild-type HIV-1 protease (WT−PR) and the unbound V82F/I84V double-mutated protease (WT−PR) with respect to the first snapshot as a function of time.

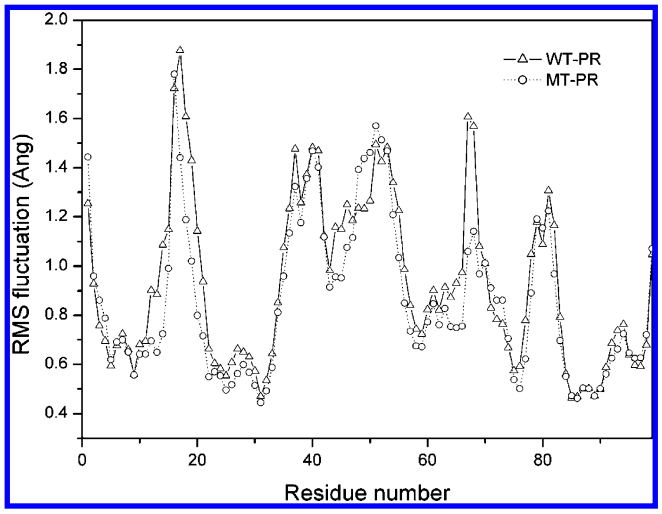

Figure 8. Root-mean-square fluctuation of backbone atoms versus residue number for both monomers of the unbound wild-type HIV-1 protease (WT-PR) and the unbound V82F/I84V double-mutated HIV-1 protease (MT-PR).

in Figure 10c (0.74 for wild-type and 0.75 for mutant) are quite smaller than those in Figure 10a (1.05 for wild-type and 1.43 for mutant) and 10b (0.87 for wild-type and 1.06 for mutant). The lower SD value of the average distance means that the flapping movement of monomer A and that of monomer B are not completely independent, and cooperative movement should exist between the flaps of monomer A and monomer B. Therefore, the flaps in monomer A and monomer B do not prefer to flap in or flap out synchronously along two opposite directions. Meanwhile, the histograms of the distributions of the average distances indicate that the wild-type's flaps and the mutant's flaps bear similar opening extent, which is indicated by the similar histogram curve and the almost identical peak points (Figure 10d).

According to experiments, the *apo* protease thermodynamically favors the semiopen form.[47] In order to investigate the opening states of snapshots in wild-type's and mutant trajectories quantitatively, the I50−D25 and the I50′−D25′ distances in the wild-type and the mutated proteases were compared with the corresponding distances in the *apo* HIV-1 protease crystal structure in the semiopen form (PDB entry: 1hhp).[58] In the crystal structure of 1hhp, the distance between the D25 C_α atom and the I50 C_a atom is 17.2 Å. In Figure 10a, it can be observed that only a small set of snapshots sampled larger D25−I50 distance than 17.2 Å. In order to visually depict the largest flap opening conformations sampled in MD simulations, the snapshots with the maximum D25−I50 distances of monomer A were aligned onto the crystal structure (Figure 11). By analyzing the alignment of the flap conformations, it can be seen that monomer A in the wild-type protease or in the mutated protease almost reaches the semiopen conformation. It should be noted that the monomer B in the wild-type protease or in the mutated protease in Figure 11 does not open enough to sample the semiopen distance value. Furthermore, in Figure 10c, we observe that the average I49−D25/I49′−D25′distance does not sample any region close to the value of 17.2 Å. So we believe that in 18 ns MD simulations, only limited snapshots reach the transient conformational space from the closed state to the semiopen state and longer MD simulations may be necessary to overcome energetic or kinetic barriers and reach the semiopen conformational space.

On the basis of the above analyses, we may make the following conclusions. First, the mutated protease is a little more stable than the wild-type protease. Second, the flaps of the mutated protease and the wild-type protease possess similar dynamics properties and opening extent. Obviously, the simulation results obtained in the current work are quite different from those reported by Perryman et al.[54] In Perryman's work, the wild-type protease seems more stable because the authors observed larger rmsd fluctuation of the mutated protease than that of the wild-type protease. But according to the scanning calorimetry experiments reported by Todd,[59] the mutated protease undergoes thermal denaturation at 4 °C higher than the wild type, which means that the mutated protease is more stable. This is consistent with our observations. Furthermore, in Perryman's work, the authors found that the mutated protease's flaps opened farther than the wild-type's flaps and displayed more flexibility. Furthermore, the authors pointed out that if "this mutant does actually prefer the semi-open conformations more than the wild type favors them, then that could be a general feature contributing to its drug resistance properties, because all the drugs would have to pay a larger enthalpic cost to close the mutant's flaps". If Perryman's assumption is correct, the difference between the flap conformations of the wild-type protease and the mutated protease will lower the affinities of

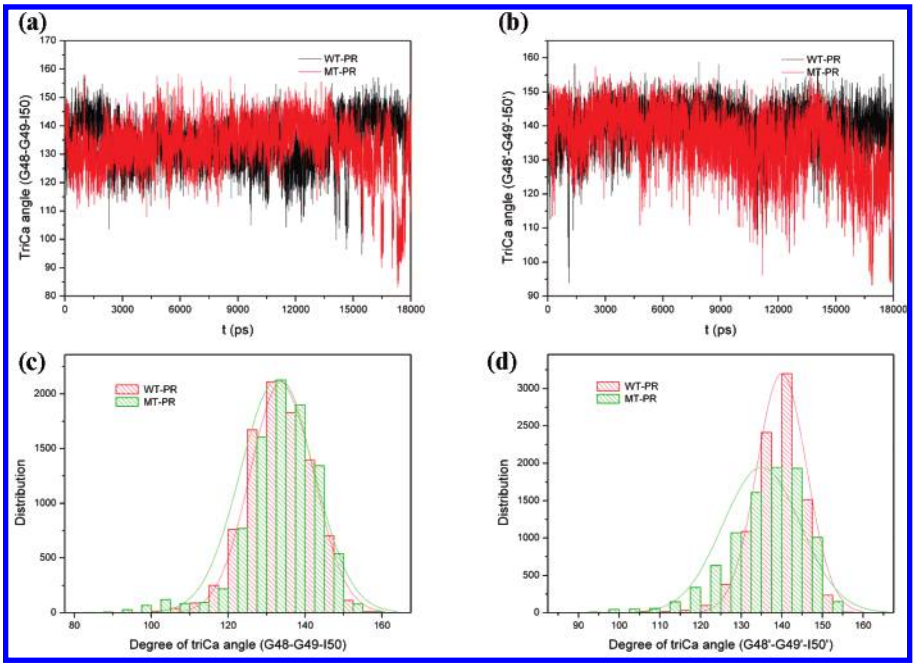

Figure 9. Variability of (a) the G48-G49-I50 triC$_\alpha$ angle and (b) the G48′-G49′-I50′ triC$_\alpha$ angle of the unbound wild-type protease (WT-PR) and the unbound mutated protease (MT-PR). Histogram distributions of (c) the G48-G49-I50 triC$_\alpha$ angle and (d) the G48′-G49′-I50′ triC$_\alpha$ angle.

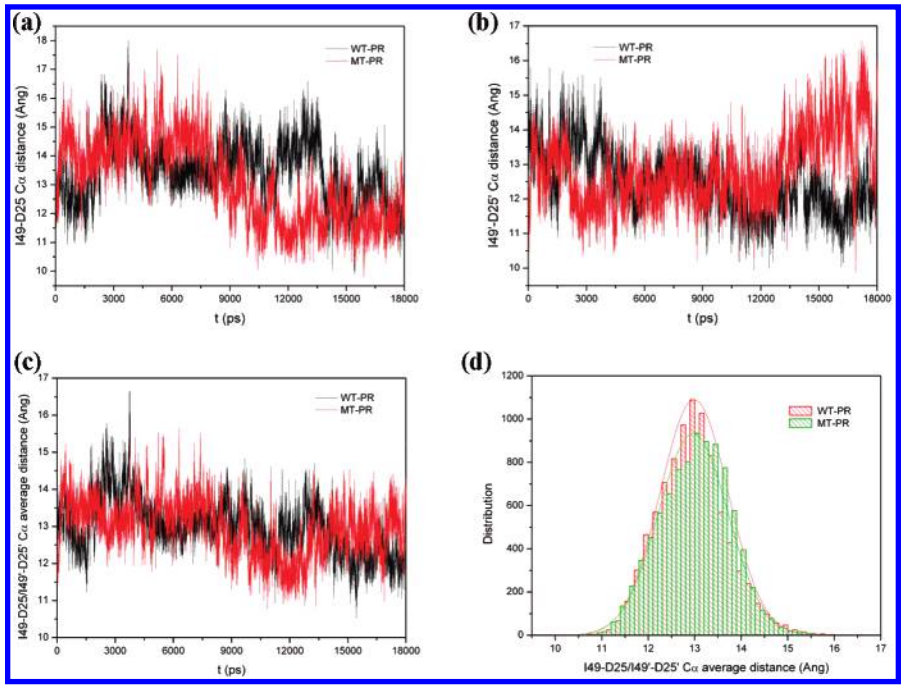

Figure 10. Variability of (a) the I49−D25 C$_\alpha$ distances, (b) the I49′−D25′ distances, and (c) the I49−D25/I49′−D25′ average distance of the unbound wild-type protease (WT-PR) and the unbound mutated protease (MT-PR). (d) Histogram distributions of the average distance in Figure 10c.

both (inhibitors and substrates) by similar amounts. Furthermore, according to the published data of K_m, the binding of the substrate caused by the V82F/I84V double mutation decreases by about 1.1 kcal/mol,[11] which is close to the value (1.4 kcal/mol) of the difference between the conformational energy of the wild-type protease and that of the mutated protease.[59] That is to say, the change of the binding of substrate is primarily caused by the change of the structural stability, not by the other factors such as the flap opening.

(iv) The Mechanisms of the Drug Resistance Caused by the V82F/I84V Double Mutation. The rmsd values for the protease backbone atoms of the mutated and the wild-type complexes relative to the starting structures were plotted in Figure S5 in the Supporting Information. As a comparison, it seems that all complexed structures can achieve good equilibrium after about 200 ps except the wild-type **1** complex. After comparison, it can be found that the rmsd values of the mutated complex and the wild-type complex do not have large differences. The comparisons of the rmsf values of the mutated complexes and those of the wild-type complexes are shown in Figure 12. Overall, the rmsf values of the mutated complex and the wild-type complex do not have large difference.

Absolute binding free energies between the inhibitors and the mutated protease based on the single-trajectory protocol are listed in Table 1. It is encouraging that the predicted binding free energies without considering entropy effect have good linear

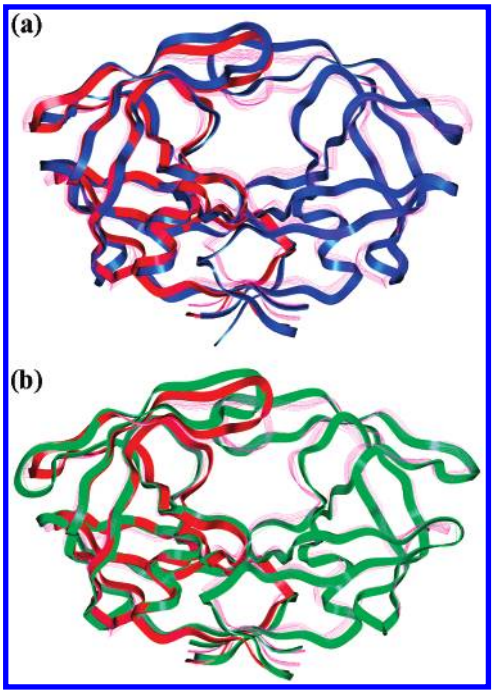

Figure 11. Comparison of snapshot with the most opening flap of monomer A of the unbound PR, the closed conformation of the protease/**1** complex, and the semiopen conformation of the 1hhp crystal structure. (a) The snapshot with the most opening flap of monomer A (3.754 ns) of the unbound wild-type PR is shown as blue solid ribbon; the closed conformation of the protease/**1** complex is shown as pink line ribbon; the semiopen conformation of 1hhp is shown as red solid ribbon. (b) The snapshot with the most opening flap of monomer A (5.234 ns) of the mutated PR is shown as green solid ribbon; the closed conformation of the protease/**1** complex is shown as pink line ribbon; the semiopen conformation of 1hhp is shown as red solid ribbon.

correlation ($r = 0.97$) with the experimental values for three wild-type complexes and two mutated complexes. If the entropy contribution was included, the correlation coefficient was decreased to 0.92. The data reported by Todd et al. show that the entropy change of the binding of indinavir, nelfinavir, saquinavir, and ritonavir led by the V82F/I84V double mutation is less than 1.0 kcal/mol.[59] Furthermore, there is also likely to be a significant systematic error in entropy prediction considering that the normal-mode analysis is based on the harmonic approximation, so the entropy effect was not considered in the discussions. According to the predicted data in Table 1, the rank of the influence of binding caused by the double mutation is **1** (3.73 kcal/mol) < **3** (3.45 kcal/mol) < **2** (2.01 kcal/mol). The affinity of **3** to the mutated protease is not reported. But according to our prediction, the binding of **3** is also sensitive to the V82F/I84V double mutation.

In order to make a full investigation of influence of the V82F/I84V double mutation to the interaction of inhibitors, the inhibitor−residue interactions in each wild-type complex and the corresponding mutated complex were decomposed and compared systematically. Figure 13 shows the subtraction between the inhibitor−residue interactions of the wild-type **1** complex and those of the mutated **1** complex (the residues with absolute difference larger than 0.75 kcal/mol were labeled). In total there are 15 residues with a large difference, in which nine are related to the decrease of **1** binding with the mutated protease and the other six are responsible for the decrease of **1** binding with the wild-type protease. It is easy to find that not all mutated residues (F82, F82′, V84, V84′) decrease the binding of **1**. Actually, only V84′ is involved in the decrease of **1** binding with the mutated protease, while F82 in the mutated protease

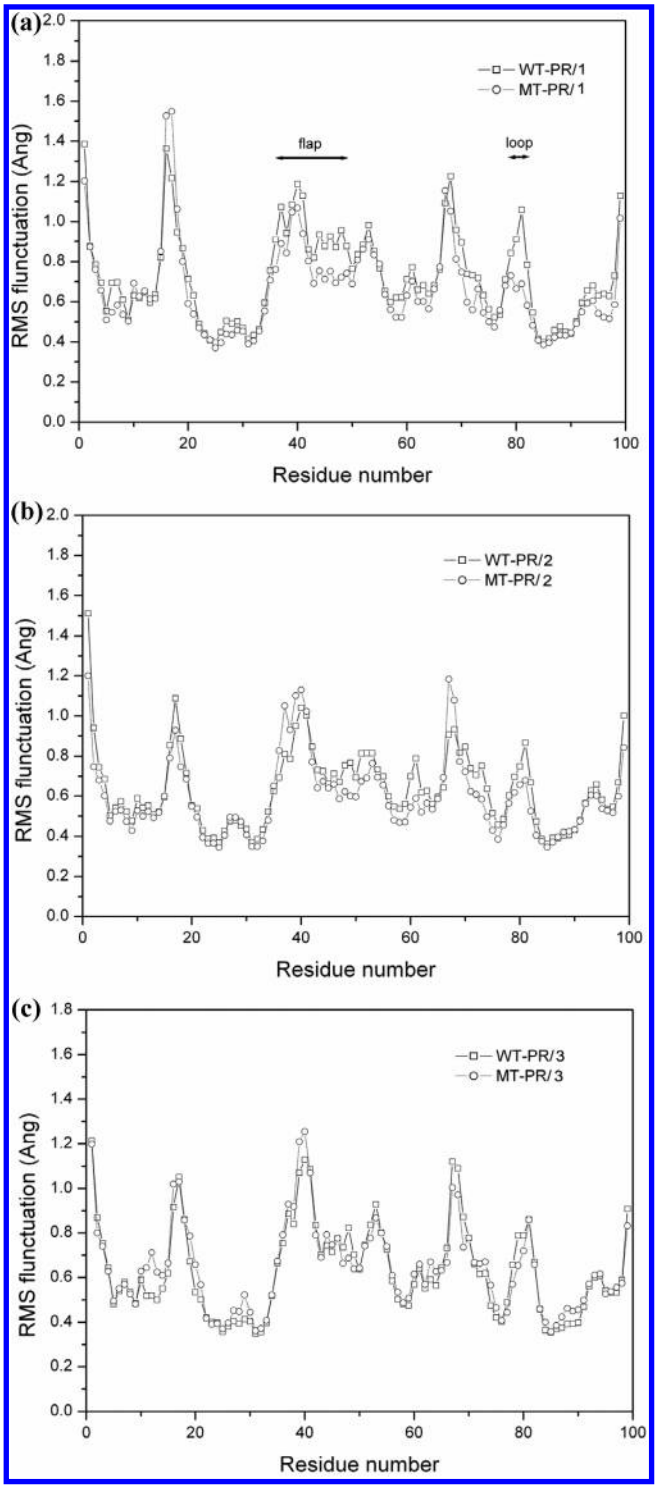

Figure 12. Root-mean-square fluctuation of backbone atoms versus residue number for both monomers of (a) the wild-type HIV-1 protease/**1** complex and the mutated HIV-1 protease/**1** complex, (b) the wild-type HIV-1 protease/**2** complex and the mutated HIV-1 protease/**2** complex, and (c) the wild-type HIV-1 protease/**3** complex and the mutated HIV-1 protease/**3** complex.

even forms stronger interaction with **1**. As shown in Figure 13, many residues in addition to the mutated residues contribute to the loss of binding (the important residues are highlighted in Figure 14a). In Figure 14a, the unfavorable and favorable residues can be roughly defined into three clusters: one unfavorable cluster at the flap regions (cluster1: Ile47, Ile50, Ile47′, and Ile50′), the other unfavorable cluster near the benzene ring of **1** (cluster2: Gly27, Asp29, Arg8′, Leu23′, and Val84′),

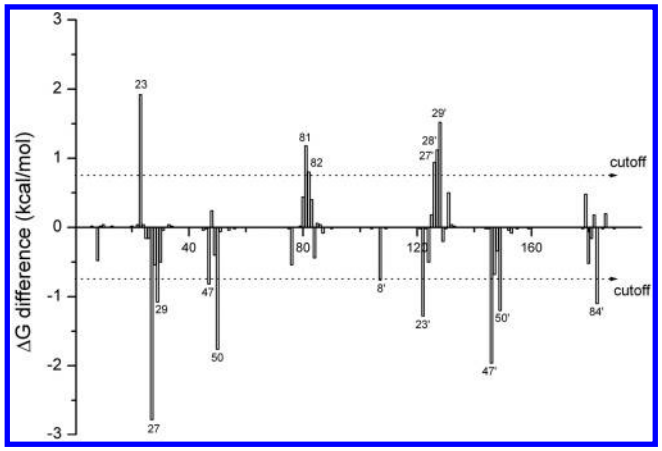

Figure 13. The distribution of the difference between the inhibitor−residue interactions of the wild-type **1** complex and those of the mutated **1** complex. The residues with absolute difference larger than 0.75 kcal/mol are labeled by two cutoff lines.

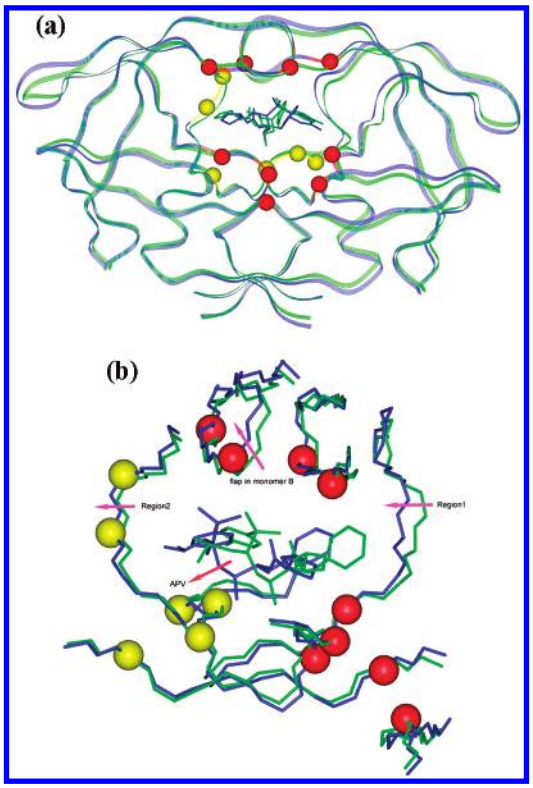

Figure 14. (a) The alignment of the average structures of the wild-type HIV-1 protease/**1** complex and the mutated HIV-1 protease/**1** complex. (b) The inhibitors and residues near the active site extracted from Figure 19a. The mutated complex was shown in blue and the wild-type complex in green. The C_α carbon atoms of the unfavorable residues to the binding of **1** are shown as the red CPK model and those of the favorable residues as the yellow CPK model. The **1** inhibitor in the wild-type complex is shown as the green stick model and that in the mutated complex as the blue stick model. The relative direction of inhibitors in the wild-type complex and the mutated complex is labeled as a red arrow, and conformational changes of region1, region2, and the flap of monomer B are labeled as pink arrows.

and one favorable cluster which is at the other side of protease to cluster2 (cluster3: Leu23, Phe82, Gly27′, Ala28′, and Asp29′).

As shown in Figure 14b, in the mutated complex the position of **1** is quite different from that in the wild-type complex. **1** in the mutated complex is a little far from cluster1 and cluster2 but closer to cluster3. We believe that the change of the position of **1** in the active site should be induced by the conformational change of the active site caused by the double mutation. Overall, two proteases shown in Figure 14a are quite similar, which is indicated by a low rmsd value of the backbone atoms (0.68). After careful observations of the superimposed structures, we found that two loop regions (region1: Gly78′ to Asn83′ in monomer B; region2: Pro79 to Asn83 in monomer A) had relatively large conformational difference in these two complexes. Compared with region1 and region2 in the wild-type complex, region1 in the mutated complex is much closer to the center of the active site, while region2 moves slightly away from the active site. The effect the conformational change of the loop regions leads to the positional adjustment of **1** between region1 and region2. As shown by the red arrow in Figure 14b, **1** is pushed away from the unfavorable cluster1 and close to the favorable cluster3. Furthermore, the position adjustment of **1** makes it move away from the flaps. In the alignment structure, the flap in monomer B of the mutated complex opens a little farther than the wild-type's flap, which may be caused by the less favorable interactions between **1** and the flaps of the mutated complex. The residue-inhibitor energy decomposition calculations were conducted on the **2** complexes and the **3** complexes, and similar distributions of the important residues and conformational changes of the active site were also observed.

Our predictions indicate that many residues in addition to the mutated residues are related to the loss of binding. Furthermore, the V82F/I84V double mutation will distort the binding site and weaken the favorable interactions of inhibitors preshaped to the wild-type binding site. It may be easier for a substrate to adapt to a geometrically distorted binding site because of its high flexibilities. So we hypothesized that the conformational transformation of the active site and the inability of the inhibitors adapting to the distorted binding site in the mutated protease lead to the drug resistance caused by the V82F/I84V double mutation.

Acknowledgment. T.J. thanks Dr. Wei Wang and Dr. William A. McLaughlin for their invaluable discussions. The computational resources of this project were provided by the Center for Theoretical Biological Physics (CTBP), the National Biomedical Computation Resource (NBCR), and the National Center for Supercomputing Applications (NCSA). We are very grateful to Prof. J. Andrew McCammon for providing access to computer software such as InsightII and SYBYL. T.H. is supported by a CTBP postdoctoral scholarship.

Supporting Information Available: Details on the processes to determine the protonation state of the **1**/wild-type protease complex and comparison of the two protocols for calculating binding free energies. This material is available free of charge via the Internet at http://pubs.acs.org.

References

(1) Wlodawer, A. Rational approach to AIDS drug design through structural biology. *Annu. Rev. Med.* **2002**, *53*, 595−614.
(2) Navia, M. A.; Fitzgerald, P. M. D.; Mckeever, B. M.; Leu, C. T.; Heimbach, J. C.; Herber, W. K.; Sigal, I. S.; Darke, P. L.; Springer, J. P. 3-Dimensional Structure of Aspartyl Protease from Human Immunodeficiency Virus Hiv-1. *Nature* **1989**, *337*, 615−620.
(3) Prabu-Jeyabalan, M.; Nalivaika, E.; Schiffer, C. A. Substrate shape determines specificity of recognition for HIV-1 protease: Analysis of crystal structures of six substrate complexes. *Structure* **2002**, *10*, 369−381.
(4) Swain, A. L.; Miller, M. M.; Green, J.; Rich, D. H.; Schneider, J.; Kent, S. B. H.; Wlodawer, A. X-Ray Crystallographic Structure of a Complex between a Synthetic Protease of Human Immunodeficiency Virus-1 and a Substrate-Based Hydroxyethylamine Inhibitor. *Proc. Natl. Acad. Sci. U.S.A.* **1990**, *87*, 8805−8809.

(5) Wlodawer, A.; Miller, M.; Jaskolski, M.; Sathyanarayana, B. K.; Baldwin, E.; Weber, I. T.; Selk, L. M.; Clawson, L.; Schneider, J.; Kent, S. B. H. Conserved Folding in Retroviral Proteases - Crystal-Structure of a Synthetic HIV-1 Protease. *Science* **1989**, *245*, 616−621.
(6) Barbaro, G.; Scozzafava, A.; Mastrolorenzo, A.; Supuran, C. T. Highly active antiretroviral therapy: Current state of the art, new agents and their pharmacological interactions useful for improving therapeutic outcome. *Curr. Pharm. Des.* **2005**, *11*, 1805−1843.
(7) Chen, R. X.; Quinones-Mateu, M. E.; Mansky, L. M. Drug resistance, virus fitness and HIV-1 mutagenesis. *Curr. Pharm. Des.* **2004**, *10*, 4065−4070.
(8) Clavel, F.; Hance, A. J. Medical progress: HIV drug resistance. *New Engl. J. Med.* **2004**, *350*, 1023−1035.
(9) D'Aquila, R. T.; Schapiro, J. M.; Brun-Vezinet, F.; Clotet, B.; Conway, B.; Demeter, L. M.; Grant, R. M.; Johnson, V. A.; Kuritzkes, D. R.; Loveday, C.; Shafer, R. W.; Richman, D. D. Drug Resistance Mutations in HIV-1. **2002**, *10*, 21−25.
(10) Ohtaka, H.; Schon, A.; Freire, E. Multidrug resistance to HIV-1 protease inhibition requires cooperative coupling between distal mutations. *Biochemistry* **2003**, *42*, 13659−13666.
(11) Klabe, R. M.; Bacheler, L. T.; Ala, P. J.; Erickson-Viitanen, S.; Meek, J. L. Resistance to HIV protease inhibitors: A comparison of enzyme inhibition and antiviral potency. *Biochemistry* **1998**, *37*, 8735−8742.
(12) Adkins, J. C.; Faulds, D. Amprenavir. *Drugs* **1998**, *55*, 837−842.
(13) Sham, H. L.; Kempf, D. J.; Molla, A.; Marsh, K. C.; Kumar, G. N.; Chen, C. M.; Kati, W.; Stewart, K.; Lal, R.; Hsu, A.; Betebenner, D.; Korneyeva, M.; Vasavanonda, S.; McDonald, E.; Saldivar, A.; Wideburg, N.; Chen, X. Q.; Niu, P.; Park, C.; Jayanti, V.; Grabowski, B.; Granneman, G. R.; Sun, E.; Japour, A. J.; Leonard, J. M.; Plattner, J. J.; Norbeck, D. W. ABT-378, a highly potent inhibitor of the human immunodeficiency virus protease. *Antimicrob. Agents Ch* **1998**, *42*, 3218−3224.
(14) Pazhanisamy, S.; Partaledis, J. A.; Rao, B. G.; Livingston, D. J. In vitro selection and characterization of VX-478 resistant HIV-1 variants. *Adv. Exp. Med. Biol.* **1998**, *436*, 75-+.
(15) Maguire, M.; Shortino, D.; Klein, A.; Harris, W.; Manohitharajah, V.; Tisdale, M.; Elston, R.; Yeo, J.; Randall, S.; Xu, F.; Parker, H.; May, J.; Snowden, W. Emergence of resistance to protease inhibitor amprenavir in human immunodeficiency virus type 1-infected patients: Selection of four alternative viral protease genotypes and influence of viral susceptibility to coadministered reverse transcriptase nucleoside inhibitors. *Antimicrob. Agents Chemother.* **2002**, *46*, 731−738.
(16) Surleraux, D. L. N. G.; Tahri, A.; Verschueren, W. G.; Pille, G. M. E.; de Kock, H. A.; Jonckers, T. H. M.; Peeters, A.; De Meyer, S.; Azijn, H.; Pauwels, R.; de Bethune, M. P.; King, N. M.; Prabu-Jeyabalan, M.; Schiffer, C. A.; Wigerinck, P. B. T. P. Discovery and selection of TMC114, a next generation HIV-1 protease inhibitor. *J. Med. Chem.* **2005**, *48*, 1813−1822.
(17) Ghosh, A. K.; Kincaid, J. F.; Cho, W. H.; Walters, D. E.; Krishnan, K.; Hussain, K. A.; Koo, Y.; Cho, H.; Rudall, C.; Holland, L.; Buthod, J. Potent HIV protease inhibitors incorporating high-affinity P-2-ligands and (R)-(hydroxyethylamino)sulfonamide isostere. *Bioorg. Med. Chem. Lett* **1998**, *8*, 687−690.
(18) Yoshimura, K.; Kato, R.; Kavlick, M. F.; Nguyen, A.; Maroun, V.; Maeda, K.; Hussain, K. A.; Ghosh, A. K.; Gulnik, S. V.; Erickson, J. W.; Mitsuya, H. A potent human immunodeficiency virus type 1 protease inhibitor, UIC-94003 (TMC-126), and selection of a novel (A28S) mutation in the protease active site. *J. Virol.* **2002**, *76*, 1349−1358.
(19) Kollman, P. A.; Massova, I.; Reyes, C.; Kuhn, B.; Huo, S. H.; Chong, L.; Lee, M.; Lee, T.; Duan, Y.; Wang, W.; Donini, O.; Cieplak, P.; Srinivasan, J.; Case, D. A.; Cheatham, T. E. Calculating structures and free energies of complex molecules: Combining molecular mechanics and continuum models. *Acc. Chem. Res.* **2000**, *33*, 889−897.
(20) Lee, M. R.; Duan, Y.; Kollman, P. A. Use of MM-PB/SA in estimating the free energies of proteins: Application to native, intermediates, and unfolded villin headpiece. *Proteins* **2000**, *39*, 309−316.
(21) Wang, W.; Kollman, P. A. Free energy calculations on dimer stability of the HIV protease using molecular dynamics and a continuum solvent model. *J. Mol. Biol.* **2000**, *303*, 567−582.
(22) Wang, W.; Kollman, P. A. Computational study of protein specificity: The molecular basis of HIV-1 protease drug resistance. *Proc. Natl. Acad. Sci. U.S.A.* **2001**, *98*, 14937−14942.
(23) Hou, T. J.; Guo, S. L.; Xu, X. J. Predictions of binding of a diverse set of ligands to gelatinase-A by a combination of molecular dynamics and continuum solvent models. *J. Phys. Chem. B* **2002**, *106*, 5527−5535.
(24) Hou, T. J.; Zhu, L. L.; Chen, L. R.; Xu, X. J. Mapping the binding site of a large set of quinazoline type EGF-R inhibitors using molecular field analyses and molecular docking studies. *J. Chem. Inf. Comput. Sci.* **2003**, *43*, 273−287.
(25) Lepsik, M.; Kriz, Z.; Havlas, Z. Efficiency of a second-generation HIV-1 protease inhibitor studied by molecular dynamics and absolute binding free energy calculations. *Proteins: Struct., Funct., Bioinf.* **2004**, *57*, 279−293.
(26) Hou, T. J.; Chen, K.; McLaughlin, W. A.; Lu, B. Z.; Wang, W. Computational analysis and prediction of the binding motif and protein interacting partners of the Abl SH3 domain. *PLoS Comput. Biol.* **2006**, *2*, 46−55.
(27) Kim, E. E.; Baker, C. T.; Dwyer, M. D.; Murcko, M. A.; Rao, B. G.; Tung, R. D.; Navia, M. A. Crystal-Structure of Hiv-1 Protease in Complex with Vx-478, a Potent and Orally Bioavailable Inhibitor of the Enzyme. *J. Am. Chem. Soc.* **1995**, *117*, 1181−1182.
(28) Bayly, C. I.; Cieplak, P.; Cornell, W. D.; Kollman, P. A. A Well-Behaved Electrostatic Potential Based Method Using Charge Restraints for Deriving Atomic Charges - the Resp Model. *J. Phys. Chem.* **1993**, *97*, 10269−10280.
(29) Frisch, M. J.; Trucks, G. W.; Schlegel, H. B.; Scuseria, G. E.; Robb, M. A.; Cheeseman, J. R.; Zakrzewski, V. G.; Montgomery, J. A. J.; Stratmann, R. E.; Burant, J. C.; Dapprich, S.; Millam, J. M.; Daniels, A. D.; Kudin, K. N.; Strain, M. C.; Farkas, O.; Tomasi, J.; Barone, V.; Cossi, M.; Cammi, R.; Mennucci, B.; Pomelli, C.; Adamo, C.; Clifford, S.; COshterski, J.; Petersson, G. A.; Ayala, P. Y.; Cui, Q.; Morokuma, K.; Malick, D. K.; Rabuck, A. D.; Raghavachari, K.; Foresman, J. B.; Cioslowski, J.; Ortiz, J. V.; Baboul, A. G.; Stefanov, B. B.; Liu, G.; Liashenko, A.; Piskorz, P.; Komaromi, I.; Gomperts, R.; Martin, R. L.; FOx, D. J.; Keith, T.; Al-Laham, M. A.; Peng, C. Y.; Nanayakkara, A.; Gonzalez, C.; Challacombe, M.; Gill, P. M. W.; Johnson, B.; Chen, W.; Wong, M. W.; Andres, J. L.; Gonzalez, C.; Head-Gordon, M.; Replogle, E. S.; Pople, J. A. Gaussian 98, Gaussian Inc.; Pittsburgh, PA, 1998.
(30) Case, D. A.; Cheatham, T. E.; Darden, T.; Gohlke, H.; Luo, R.; Merz, K. M.; Onufriev, A.; Simmerling, C.; Wang, B.; Woods, R. J. The Amber biomolecular simulation programs. *J. Comput. Chem.* **2005**, *26*, 1668−1688.
(31) Harte, W. E.; Beveridge, D. L. Prediction of the Protonation State of the Active-Site Aspartyl Residues in HIV-1 Protease Inhibitor Complexes Via Molecular-Dynamics Simulation. *J. Am. Chem. Soc.* **1993**, *115*, 3883−3886.
(32) Chen, X. N.; Tropsha, A. Relative Binding Free-Energies of Peptide Inhibitors of HIV-1 Protease - the Influence of the Active-Site Protonation State. *J. Med. Chem.* **1995**, *38*, 42−48.
(33) Piana, S.; Carloni, P. Conformational flexibility of the catalytic Asp dyad in HIV-1 protease: an ab initio study on the free enzyme. *Proteins* **2000**, *39*, 26−36.
(34) Piana, S.; Sebastiani, D.; Carloni, P.; Parrinello, M. Ab initio molecular dynamics-based assignment of the protonation state of pepstatin A/HIV-1 protease cleavage site. *J. Am. Chem. Soc.* **2001**, *123*, 8730−8737.
(35) SYBYL molecular simulation package, http://www.sybyl.com, 2004.
(36) Duan, Y.; Wu, C.; Chowdhury, S.; Lee, M. C.; Xiong, G. M.; Zhang, W.; Yang, R.; Cieplak, P.; Luo, R.; Lee, T.; Caldwell, J.; Wang, J. M.; Kollman, P. A point-charge force field for molecular mechanics simulations of proteins based on condensed-phase quantum mechanical calculations. *J. Comput. Chem.* **2003**, *24*, 1999−2012.
(37) Wang, J. M.; Wolf, R. M.; Caldwell, J. W.; Kollman, P. A.; Case, D. A. Development and testing of a general amber force field. *J. Comput. Chem.* **2004**, *25*, 1157−1174.
(38) Jorgensen, W. L.; Chandrasekhar, J.; Madura, J. D.; Impey, R. W.; Klein, M. L. Comparison of Simple Potential Functions for Simulating Liquid Water. *J. Chem. Phys.* **1983**, *79*, 926−935.
(39) Darden, T.; York, D.; Pedersen, L. Particle Mesh Ewald - an N.Log(N) Method for Ewald Sums in Large Systems. *J. Chem. Phys.* **1993**, *98*, 10089−10092.
(40) Ryckaert, J. P.; Ciccotti, G.; Berendsen, H. J. C. Numerical-Integration of Cartesian Equations of Motion of a System with Constraints - Molecular-Dynamics of N-Alkanes. *J. Comput. Phys.* **1977**, *23*, 327−341.
(41) Gilson, M. K.; Sharp, K. A.; Honig, B. H. Calculating the Electrostatic Potential of Molecules in Solution - Method and Error Assessment. *J. Comput. Chem.* **1988**, *9*, 327−335.
(42) Sitkoff, D.; Sharp, K. A.; Honig, B. Accurate Calculation of Hydration Free-Energies Using Macroscopic Solvent Models. *J. Phys. Chem.* **1994**, *98*, 1978−1988.
(43) Weiser, J.; Shenkin, P. S.; Still, W. C. Approximate atomic surfaces from linear combinations of pairwise overlaps (LCPO). *J. Comput. Chem.* **1999**, *20*, 217−230.

(44) Onufriev, A.; Bashford, D.; Case, D. A. Modification of the generalized Born model suitable for Macromolecules. *J. Phys. Chem. B* **2000**, *104*, 3712−3720.
(45) Freedberg, D. I.; Wang, Y. X.; Stahl, S. J.; Kaufman, J. D.; Wingfield, P. T.; Kiso, Y.; Torchia, D. A. Flexibility and function in HIV protease: Dynamics of the HIV-1 protease bound to the asymmetric inhibitor kynostatin 272 (KNI-272). *J. Am. Chem. Soc.* **1998**, *120*, 7916−7923.
(46) Zoete, V.; Michielin, O.; Karplus, M. Relation between sequence and structure of HIV-1 protease inhibitor complexes: A model system for the analysis of protein flexibility. *J. Mol. Biol.* **2002**, *315*, 21−52.
(47) Ishima, R.; Freedberg, D. I.; Wang, Y. X.; Louis, J. M.; Torchia, D. A. Flap opening and dimer-interface flexibility in the free and inhibitor-bound HIV protease, and their implications for function. *Structure* **1999**, *7*, 1047−1055.
(48) Zhu, Z. W.; Schuster, D. I.; Tuckerman, M. E. Molecular dynamics study of the connection between flap closing and binding of fullerene-based inhibitors of the HIV-1 protease. *Biochemistry* **2003**, *42*, 1326−1333.
(49) Prabu-Jeyabalan, M.; Nalivaika, E. A.; King, N. M.; Schiffer, C. A. Viability of a drug-resistant human immunodeficiency virus type 1 protease variant: Structural insights for better antiviral therapy. *J. Virol.* **2003**, *77*, 1306−1315.
(50) King, N. M.; Prabu-Jeyabalan, M.; Nalivaika, E. A.; Wigerinck, P.; de Bethune, M. P.; Schiffer, C. A. Structural and thermodynamic basis for the binding of TMC114, a next-generation human immunodeficiency virus type 1 protease inhibitor. *J. Virol.* **2004**, *78*, 12012−12021.
(51) Zhang, D. W.; Zhang, J. Z. H. Full quantum mechanical study of binding of HIV-1 protease drugs. *Int. J. Quantum Chem.* **2005**, *103*, 246−257.
(52) Maschera, B.; Darby, G.; Palu, G.; Wright, L. L.; Tisdale, M.; Myers, R.; Blair, E. D.; Furfine, E. S. Human immunodeficiency virus - Mutations in the viral protease that confer resistance to saquinavir increase the dissociation rate constant of the protease-saquinavir complex. *J. Biol. Chem.* **1996**, *271*, 33231−33235.
(53) Piana, S.; Carloni, P.; Rothlisberger, U. Drug resistance in HIV-1 protease: Flexibility-assisted mechanism of compensatory mutations. *Protein Sci.* **2002**, *11*, 2393−2402.
(54) Perryman, A. L.; Lin, J. H.; McCammon, J. A. HIV-1 protease molecular dynamics of a wild-type and of the V82F/I84V mutant: Possible contributions to drug resistance and a potential new target site for drugs. *Protein Sci.* **2004**, *13*, 1108−1123.
(55) Rick, S. W.; Erickson, J. W.; Burt, S. K. Reaction path and free energy calculations of the transition between alternate conformations of HIV-1 protease. *Proteins: Struct., Funct., Bioinf.* **1998**, *32*, 7−16.
(56) Freedberg, D. I.; Ishima, R.; Jacob, J.; Wang, Y. X.; Kustanovich, I.; Louis, J. M.; Torchia, D. A. Rapid structural fluctuations of the free HIV protease flaps in solution: Relationship to crystal structures and comparison with predictions of dynamics calculations. *Protein Sci.* **2002**, *11*, 221−232.
(57) Scott, W. R. P.; Schiffer, C. A. Curling of flap tips in HIV-1 protease as a mechanism for substrate entry and tolerance of drug resistance. *Structure* **2000**, *8*, 1259−1265.
(58) Spinelli, S.; Liu, Q. Z.; Alzari, P. M.; Hirel, P. H.; Poljak, R. J. The 3-Dimensional Structure of the Aspartyl Protease from the Hiv-1 Isolate Bru. *Biochimie* **1991**, *73*, 1391−1396.
(59) Todd, M. J.; Luque, I.; Velazquez-Campoy, A.; Freire, E. Thermodynamic basis of resistance to HIV-1 protease inhibition: Calorimetric analysis of the V82F/I84V active site resistant mutant. *Biochemistry* **2000**, *39*, 11876−11883.

JM0609162